Local Kondo Scattering in 4*d*-electron RuO_x Nanoclusters on Atomically-Resolved Ultrathin $SrRuO_3$ Films

Chuangye Song,[1,2‡] Tao Bo,[1,2‡], Xin Liu,[3] Pengjie Guo,[1,2] Sheng Meng,[1,2,4*] Kehui Wu,[1,2,4*]

[1]Songshan Lake Materials Laboratory, Dongguan, Guangdong 523808, China

[2]Institute of Physics, Chinese Academy of Sciences, Beijing 100190, China

[3]Swiss Light Source, Paul Scherrer Institute, Villigen 5232, Switzerland

[4]School of Physics, University of Chinese Academy of Sciences, Beijing 100049, China

Corresponding author: smeng@iphy.ac.cn; khwu@iphy.ac.cn;

[‡]These authors contributed equally to this work.

Abstract

Perovskite $SrRuO_3$ is a unique 4*d* transition metal oxide with coexisting spin-orbit coupling (SOC) and electron-electron correlation. However, intrinsic, non-reconstructed surface structure of $SrRuO_3$ has not been reported so far. Here we report an atomic imaging of the non-reconstructed, SrO-terminated $SrRuO_3$ surface by scanning tunneling microscopy/spectroscopy. Moreover, a Kondo resonant behavior is revealed in RuO_x clusters located on top of the nonmagnetic SrO surface layer. The density functional theory calculations confirm that RuO_x clusters possess localized 4*d*-elecron-involved spin moments and hybridize with the conduction electrons in the metal host, resulting in the appearance of the Kondo resonance features around the Fermi level. Our work demonstrates that artificially-engineered transition metal oxides provide new opportunities to explore Kondo physics in 4*d* multi-orbital systems.

Introduction

When a magnetic impurity is surrounded by free electrons, a realignment of the electron spins occurs below a critical temperature due to spin-electron interactions, a phenomenon known as the ‘‘Kondo effect’’[1, 2]. Kondo effect is generally accompanied by a resonance peak around zero bias voltage in scanning tunneling spectroscopies (STS).[3] The Kondo effect has been reported in a variety of material systems with strongly localized 3*d* and 4*f*-electron orbitals[4-7], including single atoms or molecules[8], quantum dots[9], and carbon nanotubes[10], etc. However, it is usually absent in less localized 4*d*/5*d* -electron systems, as these are unable to supply localized electrons appropriate for formation of “Kondo singlet”.[11] Thus it is still a fundamental issue whether Kondo effect can survive in 4*d*/5*d*-electron systems.

Perovskite $SrRuO_3$ (SRO) is a unique 4*d* transition metal oxide (TMO) with a balanced co-existence of spin-orbit coupling (SOC) and electron-electron correlation[12], strong hybridization of the Ru 4*d* and O 2*p* bands enhances the density of states at the Fermi level, resulting in ferromagnetic interactions and metallicity[13-17]. In the RuO_2-terminated SRO film of 4 monolayers thickness, antiferromagnetic surface and ferromagnetic metallic bulk can coexist[18]. However, due to its surface instability, the intrinsic structure of SRO film surface has not been understood so far. Although several surface reconstructions with different stoichiometry has been reported[19, 20], non-reconstructed atomic structure at the surface has not been achieved yet in this system[21-24], which hinders the further investigation of robust topological order states[25] and the quantum phenomena[26] to some extent.

In this work, SRO ultrathin films with SrO-termination is epitaxially grown on

$SrTiO_3$ substrate. Intrinsic, non-reconstructed surface has been revealed by atomically resolved STM images. Moreover, an emergent Kondo scattering feature is observed on RuO_x clusters located on the nonmagnetic SrO top layer by STS. The formation of a "Kondo singlet" ground state is attributed to the interaction between localized spins in RuO_x clusters and conduction electrons in the metal host. Our results provide a direct evidence of the Kondo physics in TMO with 4*d* orbitals

Sample preparation

Ultrathin SRO films were epitaxially grown on Nb-doped $SrTiO_3$ (NSTO) substrates at 700 °C by laser molecular beam epitaxy (Laser-MBE) monitored by reflection high energy electron diffraction (RHEED). The energy density was about 1 J cm^{-2} with the repetition rate of 2 Hz in the oxygen environment of 0.13 mbar during the SRO growth. The as-grown films were slowly cooled to room temperature (5 °C min^{-1}) under oxygen pressure of 100 mbar. The NSTO (001) substrates were etched with NH_4F-HF solution to preferentially remove SrO at the surface, and then annealed in constant oxygen flow at 1000 °C, which results in an atomically smooth, TiO_2-terminated surface.[27] The substrates were annealed at 700 °C for 20 minutes in ultrahigh vacuum (UHV) prior to the SRO deposition in order to volatilize surface carbon impurities and remove structural defects. As shown in Figure 1a, the *in-situ* monitored RHEED pattern of the NSTO (001) substrate before starting SRO deposition shows a high intensity Laue circle with all strong reflections, suggesting an atomically smooth surface. During the deposition, a vertical streakiness progressively formed in the RHEED pattern with increasing the SRO deposition, which is generally attributed to the presence of a smooth terraced surface. The intensity of the specular

spots during the deposition were monitored, the clear intensity oscillation indicates a layer-by-layer growth mode. It should be noted that the first period of the oscillation denotes a 1.5-unit cell growth to be self-terminated with SrO surface[28, 29]. The deposition was ended at the fifth oscillation. Thus, the high-quality SrO terminated SRO thin film with a thickness of 5-unit cell is obtained.

Results and discussion

The quality of the SRO thin film was further verified by atomic force microscopy (AFM), as shown in Figure 1b. An atomically smooth surface with clear terraces and steps was observed, and the height profile (Figure 1c) along the black line reveals a step height of ~ 3.96 Å, consistent with previous report.[15] To further examine the film crystallinity, high-resolution scanning transmission electron microscopy (STEM) measurements were performed. Atomically clean, alternative SrO and RuO_2 layers are clearly identified as shown in Figure 1d, exhibiting an abrupt interface.

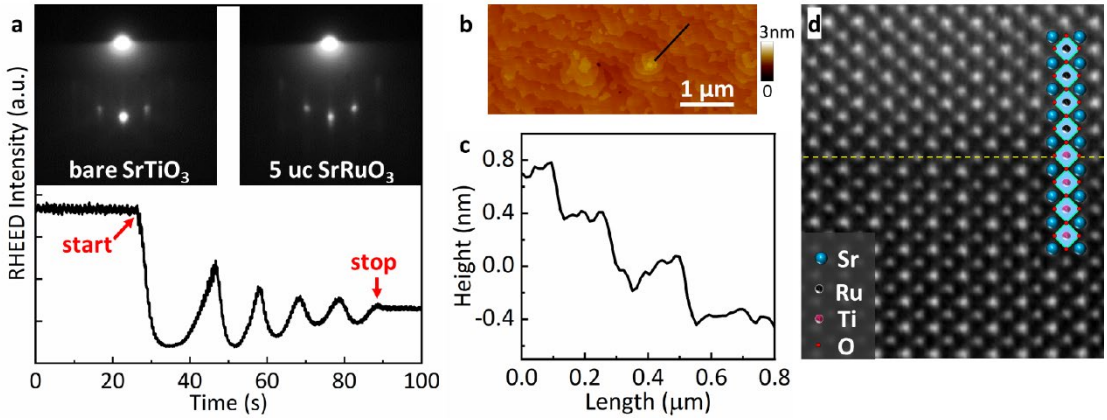

Figure 1. Epitaxial growth of SRO/NSTO thin films. (a) *In-situ* monitoring of RHEED oscillation, indicating the layer-by-layer growth of SRO film. Inset: RHEED patterns of bare NSTO and 5 uc SRO. (b) Topography of SRO thin film by AFM. (c) Height profile along the black line in (b). (d) TEM cross-section image of the SRO/NSTO thin film. The schematic shows the detail structure of the interface.

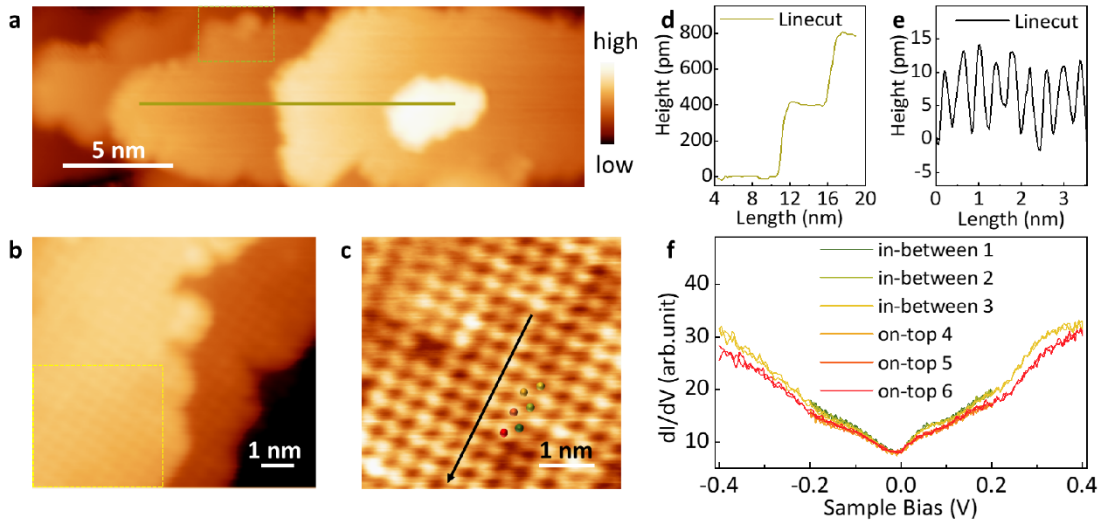

Figure 2. Atomic and electronic structure of SRO surface by STM. (a) Topographic image (V_b= 100 mV, I_t = 100 pA) of 5-unit cell thick SRO film, scale bar is 5 nm. (b) Zoom-in scan of the dark yellow dashed rectangle in (a). It should be noted that the scan angle here was rotated by 90° to obtain a high-quality imaging, and a little thermo drift occurred at the step edge during the imaging process. (c) High resolution STM images (V_b= 100 mV, I_t = 500 pA) obtained from the yellow dashed rectangle in (b), scale bar is 1 nm. (d) Line-profile along the solid line in (a). (e) Line-profile along the black arrow in (c), revealing the in-plane lattice parameters. (f) Typical dI/dV spectra measured on-top and in-between atoms, the locations are marked with colored spheres in (c).

Figure 2a shows the typical STM images with atomically flat terraces. The detailed atomic configurations shown in Figure 2b–c demonstrate a cubic structure throughout the surface. The corresponding height-profiles are presented in Figure 2d, revealing a step height of 3.96 Å. We determine the nearest neighbor surface atoms in cubic geometry arrangement is 3.91 ± 0.01Å by analyzing the line-profiles (Figure 2e). We have performed bias-dependent STM imaging, as shown in Figure S1, the as-grown SRO thin film with SrO termination was atomically resolved. The STM images with V_b= -500 mV and V_b=-50 mV exhibit almost the same atomic geometry. The corresponding calculated STM images are depicted in Figure S2c and Figure S2d

respectively, and no energy-dependent evolution of STM image is observed, suggesting a full compatibility with the experimental results (Figure S2a,b). In addition, no symmetry change is observed when changing the tip-sample distance (Figure S3). The images obtained at varied bias-voltage and height represent the accurate lattice, and indicate the absence of surface reconstructions. Differential tunneling conductance (dI/dV) curves, which are proportional to the local density of states (LDOS), have been recorded on-top and in-between atoms (see Figure 2f). The tunneling spectrum indicates a metallic electronic structure, which is in qualitative agreement with previous electrical transport measurement[30]. The LDOS in-between atoms shows very marginal difference with that of the on-top atoms, because the orbital states of sublayer RuO_2 contributes predominantly to the tunneling current in this bias voltage.[31] The changes in intensity could be attributed to the different tip height[32]. It can be seen that the energy-dependent LDOS on the terrace is periodically distributed and identical on the surface.

Interestingly, on this surface, we can find randomly distributed clusters with identical size and shape in STM images, as shown in Figure 3a. The clusters are 2 Å in height which equals to half unit cell of SRO, the lateral size of the clusters is ~ 1.2 nm in width. Here we suggest the dots to be ruthenium oxide clusters (RuO_x) based on their height and the deposition dynamics[29]. As shown in Figure S4a, X-ray photoelectron spectroscopy (XPS) was acquired at a grazing incidence angle of 5° on the ultrathin $SrRuO_3$ film. it exhibits only the $SrRuO_3$-related peaks, the observed surface stoichiometry (molar ratio) of Sr : Ru : O determined by the grazing incidence XPS spectra is about 1 : 1.08 : 3.5, which indicates the existence of excess Ru and O

atoms at the surface. No other contaminated elements are found. In addition, two doublets of Ru 3d core levels in the XPS were determined (Figure S4c): the peaks at 280.35 eV and 285.75 eV are assigned to Ru $3d_{5/2}$ and Ru $3d_{3/2}$, respectively, indicating that Ru is in the oxidation state Ru^{4+} ($SrRuO_3$). The other two small peaks at 282.35 eV and 287.35 eV correspond to $Ru^{4+\Delta}$, which is nearly in consistent with previous report[33]. For the RuO_x clusters adsorbed on the SrO-terminated $SrRuO_3$ surface, the RuO_x trends to be reoxidized compared with that beneath the SrO surface layer during the ex-situ XPS measurement. Given its relatively-weaker intensity and higher binding energy, we attribute these two small peaks to the RuO_x clusters presented at the surface due to the distinct surrounding environment in contrast to that in the bulk. Furthermore, the grazing-incidence XPS spectra of the Sr 3d core levels were also deconvoluted as shown in Figure S4d. The Sr 3d peak could be fitted by two sets of Sr $3d_{5/2}$ and Sr $3d_{3/2}$ doublets as marked with the red and blue curves. The peaks at 134.35 eV and 136 eV can be assigned to the perovskite surface termination with high-binding-energy, which is referred to as the "surface" component in this study; The low-energy component (peaks at 132.95 eV and 135.7 eV) can be assigned to the near-surface/subsurface region of the perovskite lattice, which is referred to as the "lattice" component. Such assignments are also consistent with previous works[34, 35]. The intensity of the "surface" XPS spectra is relatively stronger than that of the "lattice" in the subsurface layers, which indicates a SrO-terminated surface with a larger "surface" spectra weight.

Typical dI/dV spectra near the Fermi level (E_F) were measured precisely at the center of the RuO_x clusters. Different from the LDOS on the SrO surface, the density

of states around E_F is apparently enhanced with a resonance peak. As shown in Figure 3b, the amplitude of this peak decreases continuously and eventually vanishes when the tip is moved away from the cluster center. The resonance was observed with nearly identical height and width in more than twenty RuO_x clusters. In the RuO_x-SRO adsorption system, both the RuO_x cluster and SRO film exhibit metallic electronic structure as revealed by the dI/dV curves. Thus, we could rule out the possibility of Fermi level pining[36], which usually exists in the metal-semiconductor heterostructure. In fitting the data, we found the curves in Figure 3b can be well characterized by the Fano model. The Fano model[37] here can be described by the relation:

$$\frac{dI}{dV} \propto R(\tilde{\varepsilon}) \propto \frac{(q+\tilde{\varepsilon})^2}{1+\tilde{\varepsilon}^2}, \qquad (1)$$

where R is the transition rate, q is the interference parameter that controls the resonance shape, $\tilde{\varepsilon}$ represents the energy parameter as a function of the resonance energy and width. Here $\tilde{\varepsilon} = \frac{eV-\alpha}{\Gamma/2}$, where e is the elementary charge, α is the energy shift of the resonance center with respect to E_F, and $\Gamma = 2k_BT_K$ is the width of the resonance where k_B is the Boltzmann constant and T_K is the Kondo temperature. In order to fit the experiment data best, a constant and a nonlinear background term can be taken into account: $\frac{dI}{dV} = aR(\tilde{\varepsilon}) + bV^2 + cV + d$, (2)
Here we use the Fano model to fit the resonance at T = 77 K with parameters of $\Gamma \sim 46 \pm 4$ meV, $q \sim -3.5$, and $\alpha \sim 2.1$ meV (see Figure 3c). T_K is determined to be 77.8 K, which coincides well with the Fermi-liquid theory: $\Gamma = 2\sqrt{(\pi\kappa_BT)^2 + 2(\kappa_BT_K)^2}$. The Fano model has been successfully applied to surface Kondo systems to describe the quantum interference between a localized magnetic impurity and a continuum electronic states in the metal host.[4, 38, 39] Thus, the well fit of the asymmetric peak and

peak position by the Fano model suggests that the resonance near E_F possibly

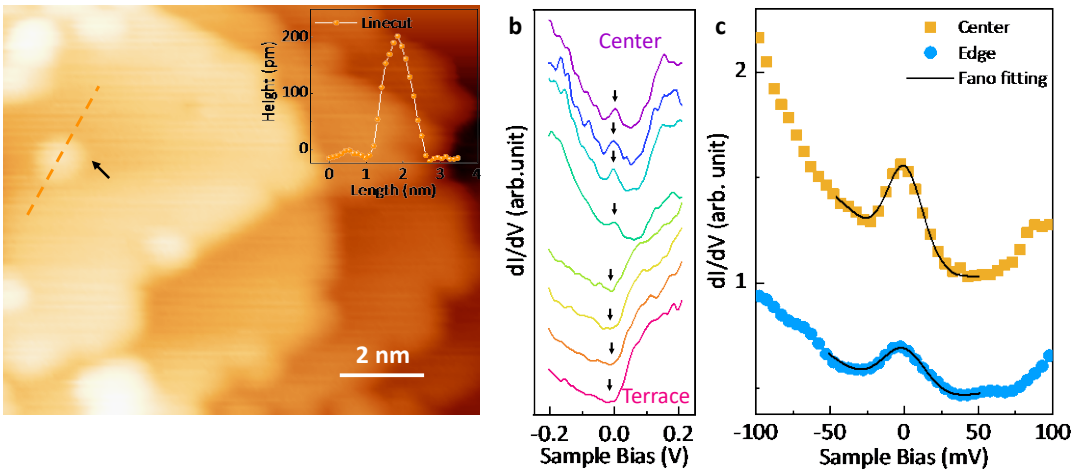

originates from the Kondo effect.

Figures 3. Kondo resonance of RuO_x clusters. (a) STM image of random distributed RuO_x clusters on SrO-terminated SRO thin film. The inset is the height profile along the red line. (b) Typical dI/dV spectra measured when moving the tip from the center of a RuO_x cluster to the SrO terrace. (c) A fit to the resonance at 77 K in (b) according to the Fano model, a constant and a nonlinear background term are taken into account here, orange and blue symbols denote experimental results.

To get insight into the microscopic origin of our experimental observations, we performed DFT calculations on the structural and electronic properties of RuO_x clusters adsorbed on SrO layer. For the sake of simplicity, we used a slab model consisting of a single RuO_x chemically bonded with SrO-layer terminated SRO in the adsorption system (see Figure 4a and 4b), another two similar slabs are present in Figure S5. We have examined the electronic structure of the adsorbed Ru atom for electron-electron interaction U=0. The Fermi energy is used as reference by setting it to zero. The up- and down-spin partial density of states are plotted in Figure 4c and 4d. The up-spin sates now move deeper into the valence band in comparison with the down-spin counterparts, and thus the RuO_x becomes spin polarized near the E_F. The

partial density of states (PDOS) of Ru atom in this adsorbed system reveals that net magnetization is produced. In comparison, the model of SrO_x-SRO adsorption system was also constructed as shown in Figure S6, no local moment was observed. Therefore, interaction between the RuO_x cluster and SrO-layer clearly changes the electronic structures and magnetic properties of the adsorbed Ru atom, which is different from the completely quenched magnet moment of free RuO_x clusters in previous report[40]. The value of T_k deduced from Figure 3c is relatively higher than the previously reported Kondo-type scattering in bulk $BaRuO_3$[41], as well as our electrical transport measurement (Figure S7).To understand the high Kondo temperature in this surface system as mentioned above, the on-site Coulomb repulsion U in 4d ruthenium oxides is relatively suppressed compared with that of 3d electron system[42], the change of U in this adsorbed Ru atom with reduced coordination number can be negligible, while the surface Ru atoms with a formal d^4 configuration in 4d-SRO exhibit quite large octahedral crystal-field splitting Δ.[18, 43] According to the theoretical modes for the Kondo temperature T_K, T_K increases monotonically as Δ increases,

$$T_K = D_0 e^{-(\pi U/8\Delta M)}, \qquad (2)$$

where D is a prefactor and M is the degeneracy number.[44, 45] Thus, ruthenate clusters possess local spin moments and couples with the conduction electrons at the surface, resulting in a robust resonant feature and high T_k.

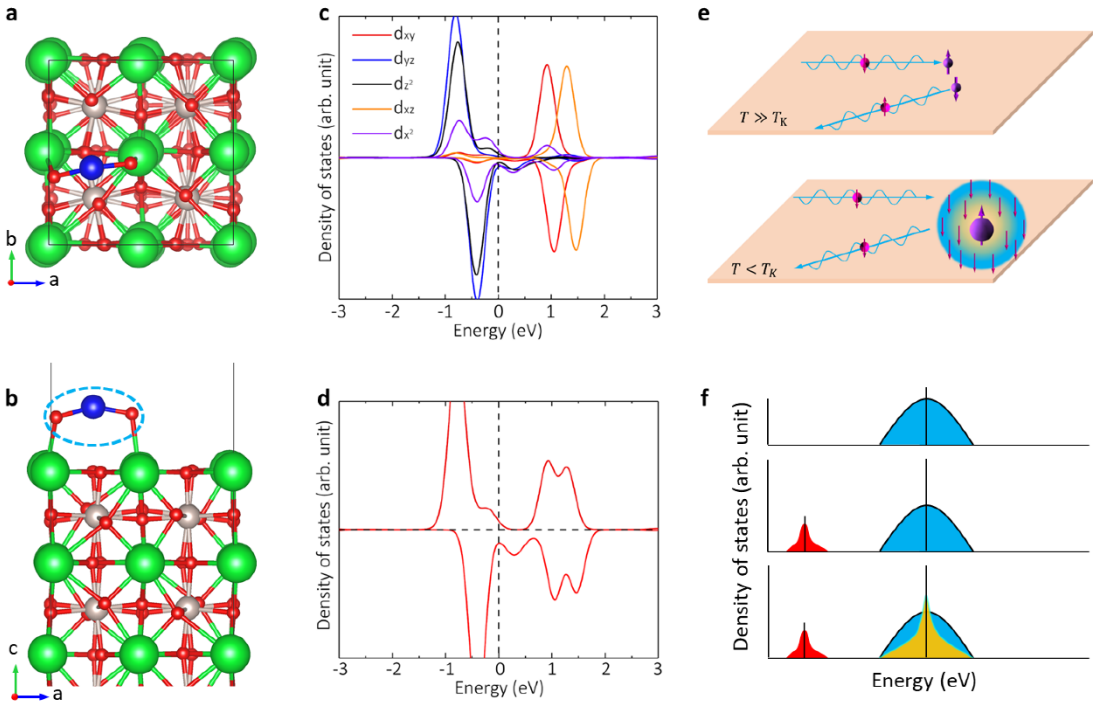

Figure 4. DFT calculations and schematic of physical mechanism. (a) and (b) Top and side views, respectively, of the optimized structure model for RuO_x-SRO adsorption system. Here we use blue atom to denote the adsorbed Ru atom. The Sr, Ru and O atoms in the bulk are denoted with green, grey and red spheres, respectively. (c) The PDOS of the adsorbed Ru atom, with 4*d*-orbital-resolved $e_g(d_{xy}, d_{yz}, d_{xz})$ and $t_{2g}(d_{x^2}, d_{z^2})$ bands. (d) The total PDOS of adsorbed Ru atom. (e) Schematic of scattering mechanism, Exchange processes can take place which flip the spin of the impurity from the "up" to the "down" state, or vice versa. (f) The singly occupied $4d^1$ state lies below the Fermi energy at ε_{4d} and is broadened by Δ due to hybridization with the conduction electron of the SrO layer. The Kondo resonance occurs at approximately E_F below T_K.

Conclusion

STM/STS studies of non-reconstructed SrO-terminated $SrRuO_3$ surface is reported for the first time here, and an emergent Kondo scattering behavior involving 4*d*-electrons is identified on a RuO_x cluster, where the localized net spin moments hybridize with the conduction electrons in the metal host, resulting in the appearance

of the Kondo resonance features around the Fermi level. This work expands the scope of Kondo effect to the artificially-engineered transition metal oxides with 4*d* orbital electrons. Furthermore, it may also shed light on the spin fluctuations in other ruthenate oxides (Sr_2RuO_4, $Sr_3Ru_2O_7$).

Materials and Methods

STM/STS measurement: The as-grown SRO thin film was *in-situ* transferred to the STM chamber (Unisoku USM1500) in UHV with a base pressure of 6.0×10^{-11} mbar. The STM experiments were performed with Pt/Ir tips at 77 K, in constant-current mode with the bias voltage (V_b) applied to the sample. STS spectrum was recorded using the lock-in technique with a bias-voltage modulation of 5 mV and 983 Hz.

XPS measurement: X-ray photoelectron spectroscopy (XPS) was performed using thermo Fisher ESCALAB Xi+ spectrometer equipped with an Al Kα monochromatic X-ray source (1486.6 eV). C 1s (284.8 eV) is used for calibration.

DFT calculations: The first-principles calculations were carried out by using the density functional theory (DFT) method, within the Perdew-Burke-Ernzerhof form of the generalized gradient approximation (PBE-GGA)[46] as implemented in the Vienna *Ab initio* Simulation Package (VASP).[47] The projector augmented wave (PAW) method[48] was used to describe the electron-ion interaction. The $SrRuO_3$ (001) surface was modeled by a periodic $p(2\times2)$ slab. *K*-points are sampled using $8 \times 8 \times 8$ and $4 \times 4 \times 1$ Monkhorst-Pack[49] meshes for the $SrRuO_3$ bulk and slab, respectively. Spin polarization is included in all the studied systems. The calculations were performed with the cutoff energy of 550 eV and the atomic positions are fully relaxed until the maximum force on each atom is less than 0.01 eV $Å^{-1}$.

Acknowledgements

This work was supported by the Ministry of Science and Technology of China (Grants No. 2016YFA0300904), National Natural Science Foundation of China (Grants No.

11825405, and No.1192780039), the Strategic Priority Research Program of Chinese Academy of Sciences (No. XDB30000000), C.S. acknowledges support from the China Postdoctoral Science Foundation (No. 2020M670502)

Author contributions: Wu K and Song C conceived the experiments and prepared the manuscript. Song C performed the STM/STS measurement. Liu X grown the samples and carried out the electrical transport measurement. Meng S and Bo T performed the DFT calculations. All authors were involved in the analysis of the experimental and theoretical results.

Competing Interest

The authors declare no competing interests.

References

1. P. W. Anderson, *Phys. Rev.*, 1961, **124**, 41-53.
2. J. Kondo, *Phys. Rev.*, 1968, **169**, 437-440.
3. M. Ternes, *New J. Phys.*, 2015, **17**.
4. A. Zhao, Q. Li, L. Chen, H. Xiang, W. Wang, S. Pan, B. Wang, X. Xiao, J. Yang and J. G. Hou, *Science*, 2005, **309**, 1542-1544.
5. T. Komeda, H. Isshiki, J. Liu, Y. F. Zhang, N. Lorente, K. Katoh, B. K. Breedlove and M. Yamashita, *Nat. Commun.*, 2011, **2**, 217.
6. A. Mugarza, C. Krull, R. Robles, S. Stepanow, G. Ceballos and P. Gambardella, *Nat. Commun.*, 2011, **2**, 490.
7. Y. S. Fu, S. H. Ji, X. Chen, X. C. Ma, R. Wu, C. C. Wang, W. H. Duan, X. H. Qiu, B. Sun, P. Zhang, J. F. Jia and Q. K. Xue, *Phys. Rev. Lett.*, 2007, **99**, 256601.
8. R. Hiraoka, E. Minamitani, R. Arafune, N. Tsukahara, S. Watanabe, M. Kawai and N. Takagi, *Nat. Commun.*, 2017, **8**, 16012.
9. M. Gaass, A. K. Huttel, K. Kang, I. Weymann, J. von Delft and C. Strunk, *Phys. Rev. Lett.*, 2011, **107**, 176808.
10. P. Jarillo-Herrero, J. Kong, H. S. J. Van Der Zant, C. Dekker, L. P. Kouwenhoven and S. De Franceschi, *Nature*, 2005, **434**, 484-488.
11. M. Kim, J. Kwon, C. H. Kim, Y. Kim, D. Chung, H. Ryu, J. Jung, B. S. Kim, D. Song and J. D. Denlinger, *arXiv preprint arXiv:2102.09760*, 2021.
12. S. Pang, *Appl. Microscopy*, 2017, **47**, 187-202.
13. P. B. Allen, H. Berger, O. Chauvet, L. Forro, T. Jarlborg, A. Junod, B. Revaz

and G. Santi, *Phys. Rev. B*, 1996, **53**, 4393.

14. A. J. Grutter, F. J. Wong, E. Arenholz, A. Vailionis and Y. Suzuki, *Phys. Rev. B*, 2012, **85**, 134429.

15. J. Lu, L. Si, X. Yao, C. Tian, J. Wang, Q. Zhang, Z. Lai, I. A. Malik, X. Liu, P. Jiang, K. Zhu, Y. Shi, Z. Luo, L. Gu, K. Held, W. Mi, Z. Zhong, C.-W. Nan and J. Zhang, *Phys. Rev. B*, 2020, **101**.

16. K. Ishigami, K. Yoshimatsu, D. Toyota, M. Takizawa, T. Yoshida, G. Shibata, T. Harano, Y. Takahashi, T. Kadono, V. K. Verma, V. R. Singh, Y. Takeda, T. Okane, Y. Saitoh, H. Yamagami, T. Koide, M. Oshima, H. Kumigashira and A. Fujimori, *Phys. Rev. B*, 2015, **92**, 064402.

17. J. Xia, W. Siemons, G. Koster, M. R. Beasley and A. Kapitulnik, *Phys. Rev. B*, 2009, **79**, 140407.

18. P. Mahadevan, F. Aryasetiawan, A. Janotti and T. Sasaki, *Phys. Rev. B*, 2009, **80**.

19. J. Shin, S. V. Kalinin, H. N. Lee, H. M. Christen, R. G. Moore, E. W. Plummer and A. P. Baddorf, *Surf. Sci.*, 2005, **581**, 118-132.

20. J. Shin, S. V. Kalinin, H. N. Lee, H. M. Christen, R. G. Moore, E. W. Plummer and A. P. Baddorf, *J. Mater. Res.*, 2004, **19**, 3447-3450.

21. H. G. Lee, L. Wang, L. Si, X. He, D. G. Porter, J. R. Kim, E. K. Ko, J. Kim, S. M. Park, B. Kim, A. T. S. Wee, A. Bombardi, Z. Zhong and T. W. Noh, *Adv. Mater.*, 2020, **32**, e1905815.

22. A. Tselev, P. Ganesh, L. Qiao, W. Siemons, Z. Gai, M. D. Biegalski, A. P. Baddorf and S. V. Kalinin, *ACS nano*, 2013, **7**, 4403-4413.

23. J. Shin, A. Y. Borisevich, V. Meunier, J. Zhou, E. W. Plummer, S. V. Kalinin and A. P. Baddorf, *ACS nano*, 2010, **4**, 4190-4196.

24. M. Moors, K. K. Adepalli, Q. Lu, A. Wedig, C. Bäumer, K. Skaja, B. Arndt, H. L. Tuller, R. Dittmann and R. Waser, *Acs nano*, 2016, **10**, 1481-1492.

25. Q. Qin, L. Liu, W. Lin, X. Shu, Q. Xie, Z. Lim, C. Li, S. He, G. M. Chow and J. Chen, *Adv. Mater.*, 2019, **31**, 1807008.

26. L. Si, O. Janson, G. Li, Z. Zhong, Z. Liao, G. Koster and K. Held, *Phys. Rev. Lett.*, 2017, **119**, 026402.

27. C. Song, X. Li, Y. Jiang, X. Wang, J. Yao, S. Meng and J. Zhang, *ACS Appl. Mater. Inter.*, 2019, **11**, 37279-37284.

28. P. Yu, W. Luo, D. Yi, J. X. Zhang, M. D. Rossell, C. H. Yang, L. You, G. Singh-Bhalla, S. Y. Yang and Q. He, *PNAS*, 2012, **109**, 9710-9715.

29. S. Kang, Y. Tseng, B. H. Kim, S. Yun, B. Sohn, B. Kim, D. McNally, E. Paris, C. H. Kim and C. Kim, *Phys. Rev. B*, 2019, **99**, 045113.

30. D. Toyota, I. Ohkubo, H. Kumigashira, M. Oshima, T. Ohnishi, M. Lippmaa, M. Kawasaki and H. Koinuma, *J. Appl. Phys.*, 2006, **99**, 08N505.

31. K. Iwaya, S. Satow, T. Hanaguri, N. Shannon, Y. Yoshida, S. I. Ikeda, J. P. He, Y. Kaneko, Y. Tokura, T. Yamada and H. Takagi, *Phys. Rev. Lett.*, 2007, **99**, 057208.

32. M. Švec, P. Mutombo, P. Shukrinov, V. Dudr and V. Cháb, *Nanotechnology*, 2005, **17**, 213.

33. M. E. Manríquez, L. E. Noreña, J. A. Wang, L. Chen, J. Salmones, J. González-

García, C. Reza, F. Tzompantzi, J. G. Hernández Cortez and L. Ye, *Inter. J. Photoenergy*, 2018, **2018**.

34. E. J. Crumlin, E. Mutoro, Z. Liu, M. E. Grass, M. D. Biegalski, Y.-L. Lee, D. Morgan, H. M. Christen, H. Bluhm and Y. Shao-Horn, *Energy & Environ. Sci.*, 2012, **5**, 6081-6088.

35. R. Gao, A. Fernandez, T. Chakraborty, A. Luo, D. Pesquera, S. Das, G. Velarde, V. Thoréton, J. Kilner and T. Ishihara, *Adv. Mater.*, 2021, **33**, 2100977.

36. R. T. Tung, *Appl. Phys. Rev.*, 2014, **1**, 011304.

37. U. Fano, *Phys. Rev.*, 1961, **124**, 1866-1878.

38. J. Li, W.-D. Schneider, R. Berndt and B. Delley, *Phys. Rev. Lett.*, 1998, **80**, 2893.

39. V. Madhavan, W. Chen, T. Jamneala, M. F. Crommie and N. S. Wingreen, *Science*, 1998, **280**, 567-569.

40. H. Mukuda, K. Ishida, Y. Kitaoka, K. Asayama, R. Kanno and M. Takano, *Phys.. Rev. B*, 1999, **60**, 12279-12285.

41. Y. A. Ying, Y. Liu, T. He and R. J. Cava, *Physical Review B*, 2011, **84**, 233104.

42. W. Witczak-Krempa, G. Chen, Y. B. Kim and L. Balents, *Annu. Rev. Condens. Matter. Phys.*, 2014, **5**, 57-82.

43. H. T. Jeng, S. H. Lin and C. S. Hsue, *Phys. Rev. Lett.*, 2006, **97**, 067002.

44. O. Újsághy, J. Kroha, L. Szunyogh and A. Zawadowski, *Phys. Rev. Lett.*, 2000, **85**, 2557-2560.

45. H. Q. Lin and J. E. Hirsch, *Phys. Rev. B*, 1988, **37**, 1864.

46. J. P. Perdew, K. Burke and M. Ernzerhof, *Phys. Rev. Lett.*, 1996, **77**, 3865-3868.

47. G. Kresse and J. Furthmuller, *Phys. Rev. B*, 1996, **54**, 11169-11186.

48. P. E. Blochl, *Phys. Rev. B*, 1994, **50**, 17953-17979.

49. H. J. Monkhorst and J. D. Pack, *Phys. Rev. B*, 1976, **13**, 5188.